Talanta 303 (2026) 129478

Contents lists available at ScienceDirect

Talanta

journal homepage: www.elsevier.com/locate/talanta

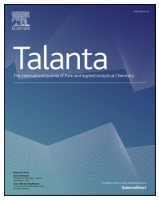

Exploring the potential of secondary resources: LA-ICP-MS for critical raw materials characterization

Debora Foppiano [a,*], Einar Jonsson [a], Sarina Bao [a], Øyvind Skår [c], Trond Slagstad [c], Pankaj Kumar [b], Maria Wallin [b], Kristina Mervič [d], Martin Šala [d], Casper van der Eijk [a]

[a] SINTEF Industry, Trondheim, Norway
[b] Norwegian University of Science and Technology (NTNU), Trondheim, Norway
[c] Geological Survey of Norway (NGU), Trondheim, Norway
[d] National Institute of Chemistry, Ljubljana, Slovenia

A B S T R A C T

This study compares methodologies and provides insights on best approaches for quantifying EU-listed critical raw materials. Europe's strategy towards greater resilience involves valorization of secondary resources such as mine tailings or by-products of metallurgical production that are typically discarded as waste, despite containing valuable resources. Thus, identifying the best methods to determine elemental concentrations in various resources is crucial for evaluating their recovery, both environmentally and economically.

Elemental content is usually determined using techniques such as inductively coupled plasma mass spectrometry (ICP-MS) by digesting solid samples into liquid solutions, although challenging for some refractory materials. Direct analysis of solids by laser ablation (LA)-ICP-MS is another alternative and can be used for both bulk analysis and spatially resolved mapping of critical elements throughout the supply value chain, from raw materials to refined products.

Here, we compare ICP-MS/MS analysis on dissolved samples, obtained after microwave-assisted acid dissolution, with LA-ICP-MS analysis on solid samples for determining rare earth element (REE) compositions of manganese ores and slags. For LA-ICP-MS, we present two approaches, particularly useful in cases where dissolution proves challenging: (i) analysis of glass beads obtained through borate flux fusion of raw powders, and (ii) direct analysis on pelletized powders using a novel non-matrix matched calibration strategy. Each method's feasibility and strengths are considered for the specific chemical composition of the samples of interests. The study shows that different methods have advantages and disadvantages related to particle size distributions and preparation costs that need to be considered during characterization of secondary resources.

1. Introduction

Secondary resources such as tailings, slags, and other by-products of mining or metallurgical production are often discarded as waste or sold as an intermediate raw material to other processes, despite containing significant amounts of valuable or critical elements [1]. Under current economic and environmental challenges, the valorization of these materials is a cornerstone of the European Union's Critical Raw Materials Act [2], which promotes circularity and sustainability in resource management.

European policies increasingly aim to reduce dependence on import of key material resources, in particular Critical Raw Materials (CRMs) [3]; some of these materials are present in secondary resources. EU listed 34 raw materials in 2023, including Mn, REEs, and others critical elements for energy technologies The HAlMan project addresses this aim by developing an integrated, low-carbon process for producing manganese-based materials for battery applications, aluminum–manganese (AlMn), and ferromanganese (FeMn) alloys using hydrogen and aluminum dross or scrap as reducing agents. Also, from the produced alumina-calcium rich slag, alumina is extracted via a hydrometallurgical step and validated as a raw material in aluminum production and the remining grey mud, CRM is extracted and the calcium rich by-product is validated in cement [4,5].

This approach aims to minimize energy consumption, increase resource efficiency, and enable the recovery of CRMs from secondary sources. A prerequisite for this process is the accurate characterization of ores and metallurgical residues to evaluate their technical and economic recovery potential.

FeMn alloys are typically produced through carbothermic reduction, where manganese oxides are reduced by mixtures of carbon and CO gas generated during the heating of Mn ores, coke, and flux in a submerged arc furnace (SAF). Industrial manganese ores exhibit considerable variation in chemical composition and physical properties, which significantly influences the efficiency and technology of Mn alloy

* Corresponding author.
E-mail address: debora.foppiano@sintef.no (D. Foppiano).

https://doi.org/10.1016/j.talanta.2026.129478
Received 10 December 2025; Received in revised form 26 January 2026; Accepted 27 January 2026
Available online 29 January 2026

production, regardless of whether reduction occurs via solid carbon or gaseous agents. Slags generated in FeMn processes also display a wide compositional range depending on the ore type. Slags with high MnO content (>25 wt%) can serve as feedstock for silicomanganese (SiMn) or high-carbon ferromanganese (HCFeMn) production, thus improving overall Mn recovery. In contrast, FeMn slags containing 8–15 wt% MnO are generally excluded from Mn alloy production and repurposed for value-added applications.

As an example, characterization of such FeMn ore and the resulting slag sources was recently carried out [6] showing that these ores can contain 660–1800 ppm of CRM, including rare earth elements (REE), whereas the produced slag can accumulate CRM up to 2300–3370 ppm.

Elemental analysis of these complex matrices is traditionally performed using techniques such as atomic absorption spectrometry (AAS), inductively coupled plasma optical emission spectrometry (ICP-OES) and inductively coupled plasma mass spectrometry (ICP-MS). These methods require complete sample dissolution, typically achieved through acid digestion, combustion, or fusion [7–10] However, dissolution introduces several drawbacks: lengthy preparation times, contamination risks, analyte loss, and incomplete recovery or dissolution from refractory minerals such as alumina or silica [11,12] These limitations hinder accurate quantification, particularly for trace elements.

Direct solid sampling techniques offer an attractive alternative by eliminating the need for dissolution and reducing sample handling. Among these, laser ablation (LA)-ICP-MS stands out for its ability to provide multi-elemental, spatially resolved analysis with minimal sample preparation. LA-ICP-MS enables simultaneous quantification of major and trace elements down to ppm levels, overcoming the limitations of X-ray fluorescence (XRF), X-ray diffraction (XRD), and energy-dispersive spectroscopy (EDS) for detecting low-mass elements (e.g., Li) and high-mass elements (e.g., PGMs) [13–16]. Unlike high-resolution imaging methods, such as focused ion beam/scanning electron microscopy (FIB/SEM), LA-ICP-MS does not require ultra-high vacuum or conductive coatings, making it operationally versatile.

Laser–sample interactions at certain wavelengths can cause non-stoichiometric ablation, leading to volatility-driven elemental fractionation. Nevertheless, stoichiometric ablation is often achievable by carefully optimizing laser parameters for the specific material. The commonly used fractionation index (FI)—the ratio of the second half of a signal to the first—reflects how elemental signals evolve as a crater deepens under a given set of conditions, which depend on a complex interplay of wavelength, fluence, pulse duration, repetition rate, scan speed, and plasma dynamics. Because each material responds differently, selecting appropriate laser settings and controlling crater geometry can minimize preferential vaporization and fractionation [17–19].

Even when ablation is not perfectly stoichiometric, quantitative accuracy in LA-ICP-MS hinges on calibration, where standards and samples ablate similarly using matrix-matched standard reference materials (SRMs). Effectively, each mineral would need to have its own SRM to be accurately determined [20–22], but such SRMs are often unavailable There are also special cases where a sum normalization approach can be used and lately a new approach of non-matrix matched calibration with normalization to the ablated volume was established [23,24]. This makes the LA-ICP-MS a powerful technique and overcomes the last drawback (i.e. calibration/accurate quantification). Of course, one needs to be prudent and take care when choosing the reference material, setting the LA fluence and in the preparation of the sample itself.

This study presents an inter-laboratory comparison of analytical strategies for CRM analyses in Mn-rich ores and metallurgical slags potentially enriched in REE (i.e., La, Ce, Pr, Nd, Sm, Eu, Gd, Tb, Dy, Ho, Er, Tm, Yb, Lu, Y). We compare ICP-MS/MS analysis of dissolved samples obtained via microwave-assisted acid digestion with LA-ICP-MS applied directly to solids. For LA-ICP-MS, two approaches are evaluated: (i) analysis of glass beads produced by borate flux fusion and (ii) direct analysis of pelletized powders using a novel non-matrix-matched calibration protocol. Each method is assessed for feasibility, accuracy, and suitability for complex sample compositions. Considering recent join European efforts towards resilience, detailed characterization of primary and secondary sources is essential to assess the technical and economic feasibility of recovering CRMs. These findings aim to guide the selection of robust analytical workflows for CRM characterization in challenging matrices, supporting resource recovery and circular economy objectives.

2. Methodology

2.1. Samples of interests

Mn ores included Nchwaning lump, Zambian lump, and two standard reference materials with similar chemical composition provided by Mintek (SARM 16 and SARM 17). The slag samples studied here were dominantly of three types. The first type comprised slags generated by aluminothermic reduction of Nchwaning lump (slag 1 and 2 produced in lab furnace at NTNU; details about the aluminothermic reduction and the produced slag has been reported elsewhere [25]). Type 2 was the HCFeMn slag (slag 3, produced at industrial scale by an industrial partner in the HAlMan consortium) and type 3 was the SiMn slag (slag 4, produced at industrial scale by an industrial partner in the HAlMan consortium).

2.2. XRF

Major elements were determined using X-ray fluorescence (XRF) spectroscopy with a Bruker AXS S4 Pioneer instrument, applying the fused bead method by an external laboratory (Nemko Norlab, Norway). Before chemical analyses, the samples were dried at 105 °C for 1 h in a laboratory air furnace, then placed in a desiccator for 10 min prior to weighing. Finally, samples were stored in sealed glass containers to minimize exposure to air.

2.3. ICP-MS/MS

Ore and slag samples available as powders were digested using microwave-assisted acid decomposition in a Milestone UltraWAVE system, employing a mixture of HF, HNO_3, and HCl (Merck, Darmstadt, Germany). The temperature program included a fast temperature ramp to 110 °C, followed by a slower increase (2.5 °C min^{-1}) to the final temperature of 180 °C, held for 60 min before the cooling step. Following dilution, elemental analysis was carried out with an Agilent 8800 Triple Quadrupole ICP-MS/MS equipped with an SPS 4 autosampler, located at SINTEF, Trondheim. The collision/reaction cell operated both in mass-shift and on-mass modes to effectively minimize isobaric and polyatomic interferences (Table 1, reporting instrumental conditions). Quantification of target elements was based on a seven-point calibration curve prepared from either single or multi-element standards (Inorganic Ventures, Virginia, USA), using ^{115}In as the internal standard. Method accuracy for microwave-assisted acid dissolution of powders was verified through standard reference materials SARM 16 (Wessels-type ore) and SARM 17 (Mamatwan-type ore) supplied by Mintek. The same standard reference materials were considered in the other methodologies simply as samples of interests, as certified values are valid only for this specific method.

Instrumental precision and accuracy were monitored throughout the analyses using quality control solutions, and reproducibility was assessed by testing at least 3 different replicates per sample. Limits of quantification (LOQ) for this method vary by element at SINTEF, ranging from 0.01 to 1.6 ppm (see Table S3, in SI). Additional details regarding the methodology were reported in a previous publication [6]. In this study, the REE considered include Y, La, Ce, Pr, Nd, Sm, Eu, Gd, Tb, Dy, Ho, Er, Tm, Yb, and Lu. The same analytical procedure was used for glass beads obtained from borate fusion.

Table 1
ICP-MS instrumental parameters.

ICP-MS	
Instrument	Agilent 8800 triple quadrupole with integrated sample introduction system for high-speed sample uptake and rapid washout
Plasma power	1500 W
Auxiliary gas flow	0.9 l min^{-1} (Ar)
Carrier gas	1.05 ml min^{-1} (Ar)
Experiment	**Acid dissolved powders**
Measurement mode	Reaction (mass-shift)
Reaction gas flow	4 ml min^{-1} (10 % O_2/He)
Measured isotopes	^{115}In, ^{139}La, ^{140}Ce, ^{141}Pr, ^{146}Nd, ^{147}Sm, ^{153}Eu, ^{157}Gd, ^{159}Tb, ^{163}Dy, ^{165}Ho, ^{166}Er, ^{169}Tm, ^{172}Yb, ^{175}Lu, ^{89}Y
Dwell times	100 ms for all isotopes
	Acid dissolved glass beads
	Reaction (mass-shift)
	4 ml min^{-1} (10 % O_2/He)
	^{115}In, ^{139}La, ^{140}Ce, ^{141}Pr, ^{146}Nd, ^{147}Sm, ^{153}Eu, ^{157}Gd, ^{159}Tb, ^{163}Dy, ^{165}Ho, ^{166}Er, ^{169}Tm, ^{172}Yb, ^{175}Lu, ^{89}Y
	100 ms for all isotopes

2.4. LA-ICP-MS on glass beads

The sample material was fused with lithium tetraborate ($Li_2B_4O_7$, Merck, Darmstadt, Germany) to form a glass bead (see Fig. S2 supporting info). Glass beads prepared from the sample, calibration standards, and control standards were analyzed at the Geological Survey of Norway using a Teledyne-Cetac Analyte Excite Excimer 193 nm laser equipped with a HelEx II two-volume cell coupled with an Agilent 8900 triple quadrupole (QqQ)-ICP-MS used in single-quad mode. The ablated material is carried by He gas into a mixing chamber, where Ar gas is introduced. The combined stream is then transferred to an ICP-MS, where the material is ionized and analytes resolved according to their mass-to-charge ratio. The measurement conditions were optimized for an oxide ion ratio less than 0.2 % $^{232}Th^{16}O^+/^{232}Th^+$. ^{6}Li was used as internal standard as developed and described in previous publications [26–28] and the external calibration was built using 8 different calibration standards (GSP-2, MA-N, G-3, STM-1, ZW-C, Sy-2, REE-1 and IF-G diluted 1:10 with pure quartz), while MAG-1 and in-house standards were used for quality control. Detailed instrumental conditions are reported in Table 2 and in Table S4 in SI.

Analyses are conducted on samples annealed at 1000 °C, and the final analytical results are recalculated from the annealed state back to the original condition of the received sample.

2.5. LA-ICP-MS on pressed powder pellets

Powders were pressed into pellets with a hydraulic press using a mold of 13 mm in diameter and applying a pressure of 10 kN, without use of any binding agents. The pellets were secured with double-side tape onto microscopy slides and introduced with the sample holder into the Helex-II chamber, optimized for fast wash-out of ablated particles and high transport efficiency [29]. The optimal configuration of carrier and makeup gases was established through laser ablation of NIST 610 silicate glass. The procedure was designed to maximize the signal intensity of $^{238}U^+$ while maintaining the ratio $^{238}U^+/^{232}Th^+$ close to unity and ensuring that $^{232}Th^{16}O^+/^{232}Th^+$ remained below 0.2 %. Each analytical run consisted of approximately 20 s of background acquisition, followed by sample data collection and an additional 20 s of purge time prior to the subsequent measurement. To minimize transient effects, signals recorded during the initial and final 5 s of the ablation sequence were excluded from integration.

Four different areas were selected across the sample (see Fig. 1) to obtain representative elemental maps (see Fig. 2). Each area was sampled through 5 consecutive lines, each 800 μm long, equally spaced and using a beam size of 20 μm. Detailed instrumental conditions are reported in Tables 2 and in Table S5 in SI, the laser parameters were set for the best image quality.

Two different sets of calibration standards were utilized for building the different calibration curves [30]:

- commonly accessible standard reference materials (SRMs), such as NIST 612 and NIST 610 glass standards,
- microanalytical reference materials (MRMs) as nano particulate (NP) pressed pellets provided by myStandards GmbH (original powders NOD-A1 -USGS-, OREAS-24b).

A 3D optical interference microscope (Zegage PRO HR, Zygo Corporation, Middlefield, CT) was used to determine the ablation volumes of the ablated area scans in samples and standards. The 3D information was recorded using a 50X magnification objective lens with a lateral resolution of 0.173 μm and a surface topography repeatability of ≤3.5 nm. The surface topography data were processed using the Mx™ software (v. 8.0.0.23, Zygo Corporation, Middlefield, CT)

Table 2
Operating conditions for LA-ICP-MS.

LA-ICP-MS analysis pressed powder		LA-ICP-MS analysis glass beads	
Laser ablation system	Teledyne CETAC - Model Analyte Excite - Excimer Laser (193 nm)	Laser ablation system	Teledyne CETAC - Model Analyte Excite - Excimer Laser (193 nm)
Energy density	3 (J cm^{-2})	Energy density	6 (J cm^{-2})
Repetition rate	50 (Hz)	Repetition rate	20(Hz)
Spot size (μm)	20	Spot size (μm)	85
Line lenght	800 μm·x 4, spaced by 40 μm (repeated in 4 different areas in the samples)	Line lenght	300 μm
ICP-MS instrument	7900 Agilent	ICP-MS instrument	8900 Agilent
RF power (W)	1550	RF power (W)	1200
Auxiliary gas	0.9 (mL·min^{-1})	Auxiliary gas	0.9 (mL·min^{-1})
Carrier gas	1.05 (mL·min^{-1})	Carrier gas	0.82(mL·min^{-1})
Dwell time	5 ms per isotope	Dwell time	5 ms per isotope
Measured isotopes	^{139}La, ^{140}Ce, ^{141}Pr, ^{146}Nd, ^{147}Sm, ^{153}Eu, ^{157}Gd, ^{159}Tb, ^{163}Dy, ^{165}Ho, ^{166}Er, ^{169}Tm, ^{172}Yb, ^{175}Lu, ^{89}Y	Measured isotopes	^{139}La, ^{140}Ce, ^{141}Pr, ^{146}Nd, ^{147}Sm, ^{153}Eu, ^{157}Gd, ^{159}Tb, ^{163}Dy, ^{165}Ho, ^{166}Er, ^{169}Tm, ^{172}Yb, ^{175}Lu, ^{89}Y

2.6. Limit of quantification comparison among techniques

The determination of limits of quantification (LOQ) remains an area without universal consensus, particularly when comparing ICP-MS and LA-ICP-MS methodologies. To enable a more consistent evaluation across techniques, the lower limit of quantification (LLQ) was instead employed, defined as the standard deviation of ten consecutive measurements of the lowest-concentration standard. A summary of LLQ values for all investigated methodologies is provided in Table S3–S5 of the Supporting Information.

Both LA-ICP-MS approaches yield LOQ values that are broadly comparable to those obtained by conventional ICP-MS. This agreement is particularly striking for pressed pellets, given that the LOQ is defined at the pixel level, where substantially less material is delivered to the plasma. These observations indicate that in this study the choice of analytical strategy will not be primarily driven by large differences in figures of merit. Instead, it should be governed by practical and methodological considerations such as particle size, sample preparation requirements, operational costs, and analytical objectives.

2.7. Data processing

Data processing and statistical analysis were performed using a combination of specialized software and Python-based workflows. Initial data selection and organization were partially carried out in Microsoft Excel; while pre-processing and reduction of LA-ICP-MS data were carried out using HDIP (Teledyne Technologies, CA, USA) and Iolite software - multi-standard calibration using the *3-D Trace Elements* module- (Elemental Scientific Lasers, NE, USA). Subsequent data manipulation, statistical evaluation and visualization were implemented in Python (Visual Studio Code environment) employing libraries such as *pandas* for data manipulation, *numpy* and *scipy* for numerical and statistical computations. Graphical outputs were generated with *matplotlib* and *seaborn*. This integrated approach ensured robust data handling, reproducible statistical analysis, and high-quality visual representation of results.

3. Results and discussion

3.1. XRF analysis

XRF analysis was included to obtain relevant information of the main matrix composition and evaluate their potential effect for interferences management in the determination of REE. XRF results are available in Tables S1 and S2 in the supporting information (SI). Zambian ores generally contain higher levels of MnO_2, and BaO (10 wt%) compared to Nchwang ores, which have generally lower BaO content (0.3 wt%). Standard reference materials SARM 16 and SARM 17, supplied by Mintek, were included for cross-validation as their compositions closely match those of the studied ores and because REE concentration data is available from previous publications [31]. For the present set of samples, Mn slags exhibit a stable compositional range, especially regarding CaO (27–38 wt%), while SiO_2 content is remarkably higher in slag 3 and 4 (44–45 wt%).

3.2. ICP-MS

Microwave-assisted acid digestion of the powders initially required substantial optimization already described in a previous publication [6], as several acid mixtures were tested before achieving satisfactory performance. In contrast, borate–silica fusion beads dissolved far more efficiently, providing a robust alternative for samples that are otherwise difficult to digest. Results for the selected Mn ore and its corresponding slag, previously reported in earlier work [6], are incorporated here in Tables 3 and 4 to support the methodological comparison.

The optimized acid mixture ultimately achieved near-complete

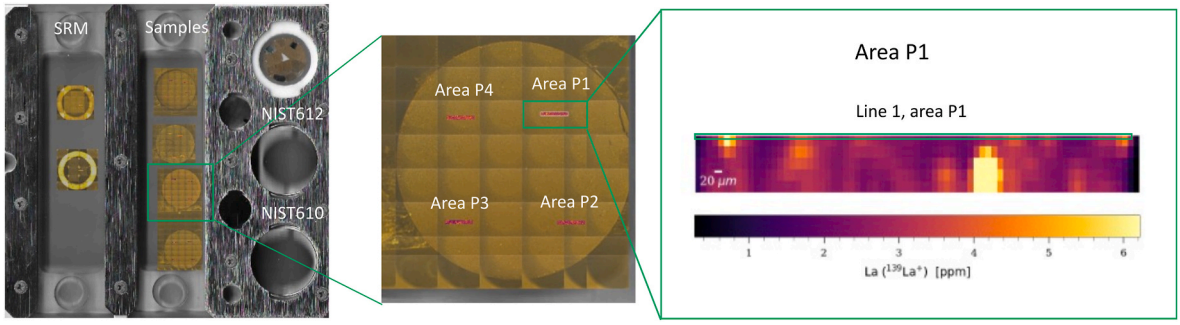

Fig. 1. LA-ICP-MS schematic summarizing the different steps of the direct sampling of pressed pellets. On the outer left the sample holder and samples positions are visible, in the center one of the samples is shown together with the 4 sampling areas P1 to P4, and on the right an example of the 2D visual representation of La concentration is shown.

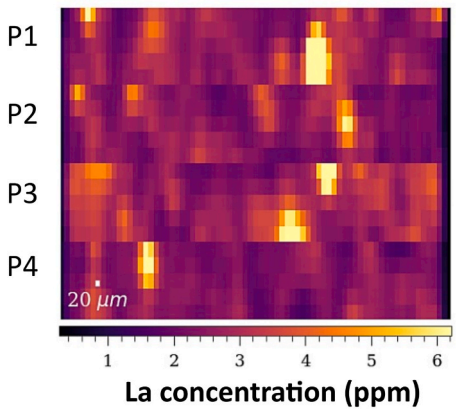

Fig. 2. LA-ICP-MS elemental map for lanthanum (La) combining the four areas (P1, P2, P3, P4), each constructed by ablating five equally spaced lines in sample SARM 17.

dissolution for most samples, although Slag 3 and Slag 4 exhibited incomplete digestion, likely due to their elevated SiO_2 content. Even so, recoveries for the targeted elements—including the rare earth elements—remained satisfactory when compared to other approaches. This suggests that the residual undissolved material is predominantly silica.

3.3. LA-ICP-MS glass beads

Analyses of REE and trace elements in geological samples by LA-ICP-MS in glass beads is a well-established method at the Geological Survey of Norway. A key benefit is that the method uses the same glass beads prepared for XRF analysis, removing the need for any additional sample preparation. Mn ores and slag results in Table 5 and 6 show consistency with ICP-MS results and satisfactory level of uncertainty Laser ablation under dry plasma conditions results in low interferences from oxide formation. Elements such as Si, Ca and Ba can be used as internal standards, but Li from lithium tetraborate is the preferred internal standard for this method. The approach has also demonstrated strong accuracy and precision, as evidenced by its performance in international proficiency testing programs for geological samples.

3.3.1. LA-ICP-MS on pressed pellets, "the naive approach"

The output of LA-ICP-MS on pressed powder are 2D elemental maps showing elemental distribution across the 4 different sampled areas P1 to P4, with a spatial resolution of 20 µm (Fig. 3). Each area is the sum of 5 different ablation lines of the same length.

Even though concentrations fluctuate across the samples, an average value can be considered to compare these results with the other methodologies (see Tables 7 and 8).

In the case of analysis of pressed pellets with LA-ICP-MS, one can see that the quality of ablated craters varies significantly with sample properties, in particular their particle size distributions (Fig. 3). Where samples of finely ground powders are used for preparation of pellets, the quality of craters after ablation are not far from the ones in NIST 610 SRM, considered as a benchmark in many LA-ICP-MS studies.

Crater morphology—defined by the shape, depth, and surface characteristics of the ablation pit—provides a direct measure of laser–sample interaction and aerosol transport efficiency. Ideally, static spot ablation produces a well-defined crater with steep walls, a flat base, and minimal melting or redeposited ejecta. Crater quality strongly influences

Table 3
ICP-MS results of Mn ores samples, using glass beads. Concentrations (C) are expressed in ppm (mg kg-1) with relative standard deviation expressed in %.

REE	Nchwaning lump		Zambian lump		SARM 16		SARM 17	
	C (mg kg^{-1})	RSD %	C (mg kg^{-1})	RSD %	C (mg kg^{-1})	RSD %	C (mg kg^{-1})	RSD %
Y	13.74	2.13	50.31	0.68	12.00	1.13	7.59	4.54
La	6.55	0.91	32.73	1.25	6.92	4.22	4.39	1.63
Ce	8.64	0.33	98.56	0.58	8.73	2.16	4.84	1.75
Pr	1.13	2.12	12.42	0.91	1.15	0.90	0.76	3.22
Nd	4.98	1.20	53.65	1.81	4.92	5.86	3.22	5.68
Sm	1.13	4.28	15.47	2.60	1.09	12.89	0.63	7.83
Eu	0.40	14.10	6.35	2.07	0.47	6.27	0.16	5.14
Gd	1.36	4.81	13.68	2.95	1.25	5.34	0.86	3.88
Tb	0.22	3.19	2.06	2.11	0.19	9.73	0.13	2.70
Dy	1.48	2.93	11.85	1.58	1.29	1.28	0.84	6.62
Ho	0.37	4.03	2.24	0.86	0.32	3.23	0.21	5.82
Er	1.16	2.24	5.84	4.37	0.91	3.60	0.62	3.88
Tm	0.26	8.27	0.90	2.18	0.23	6.33	0.20	5.62
Yb	1.14	7.59	6.01	1.68	0.92	5.60	0.66	10.57
Lu	0.20	7.22	0.75	0.74	0.17	5.66	0.11	12.78

Table 4
ICP-MS results of slag samples, using glass beads. Concentrations (C) are expressed in ppm (mg kg-1) with relative standard deviation expressed in %.

REE	Slag 1		Slag 2		Slag 3		Slag 4	
	C (mg kg^{-1})	RSD %	C (mg kg^{-1})	RSD %	C (mg kg^{-1})	RSD %	C (mg kg^{-1})	RSD %
Y	14.68	1.16	14.47	0.20	35.09	0.21	31.32	0.46
La	7.74	1.73	7.59	1.70	29.73	0.73	26.76	1.16
Ce	10.77	1.01	8.08	0.58	64.85	0.83	54.15	0.95
Pr	1.28	1.83	1.22	0.58	6.70	0.45	5.93	1.34
Nd	5.53	3.97	5.44	3.48	27.51	0.77	23.02	1.16
Sm	1.19	13.92	1.05	17.43	5.93	0.59	5.08	5.48
Eu	0.35	5.41	0.32	3.14	1.30	11.58	1.01	10.34
Gd	1.50	1.44	1.41	2.90	5.96	2.38	4.90	1.99
Tb	0.22	2.09	0.21	2.31	0.93	0.20	0.75	1.53
Dy	1.56	3.24	1.56	2.32	5.82	2.26	4.88	3.09
Ho	0.39	3.72	0.39	1.34	1.22	2.02	1.03	1.03
Er	1.21	3.78	1.18	3.30	3.65	0.34	3.10	2.85
Tm	0.27	1.16	0.27	3.57	0.60	1.47	0.52	2.32
Yb	1.19	4.57	1.21	5.91	3.42	5.68	3.23	2.65
Lu	0.20	1.49	0.19	1.68	0.52	1.75	0.46	1.13

Table 5
LA-ICP-MS results of Mn ores samples, using glass beads. Concentrations (C) are expressed in ppm (mg kg-1) with relative standard deviation expressed in %.

REE	Nchwaning lump		Zambian lump		SARM 16		SARM 17	
	C (mg kg^{-1})	RSD %	C (mg kg^{-1})	RSD %	C (mg kg^{-1})	RSD %	C (mg kg^{-1})	RSD %
Y	14.00	2.55	53.00	2.72	13.00	3.60	7.42	3.13
La	6.19	2.25	30.70	2.30	6.81	3.11	4.14	3.10
Ce	7.48	2.36	85.20	2.28	8.34	3.19	4.13	3.16
Pr	0.99	2.57	10.30	2.35	1.07	3.80	0.65	3.92
Nd	4.31	2.82	46.70	2.21	4.64	4.00	2.80	3.97
Sm	0.88	5.10	12.30	2.57	0.86	8.09	0.52	8.47
Eu	0.25	5.72	2.95	2.86	0.25	6.76	0.13	8.68
Gd	1.17	4.03	11.70	2.49	1.14	5.20	0.67	6.23
Tb	0.19	5.07	1.84	2.70	0.18	7.57	0.11	6.23
Dy	1.25	4.31	10.20	2.82	1.19	5.80	0.71	5.99
Ho	0.32	3.64	2.03	3.00	0.29	5.33	0.19	5.45
Er	0.89	4.49	5.14	2.78	0.79	5.39	0.50	6.52
Tm	0.16	5.42	0.72	3.77	0.15	7.68	0.12	7.65
Yb	0.87	5.81	4.33	3.39	0.83	7.28	0.51	8.64
Lu	0.15	4.95	0.64	3.51	0.14	7.49	0.09	7.40

analytical performance: uniform pits promote stable signals and reproducible material removal, whereas irregular or conical craters increase depth-dependent fractionation and bias elemental ratios, particularly for volatile species. Morphology also serves as a practical diagnostic for tuning fluence and repetition rate, as insufficient energy yields shallow, irregular craters and poor sensitivity, while excessive energy can damage the sample surface. Maintaining appropriate crater characteristics is therefore essential, especially when microstructural integrity must be preserved.

In the cases where coarse powders were used (slag samples, see Fig. 3c), the ablation becomes much less reproducible for the reasons stated above and it is therefore to be expected that the signal will have much higher RSD. Heterogeneity in the material might also be connected to different properties (i.e. hardness), resulting in a plume with bigger particles. It is known that the bigger particles do not get decomposed and ionized completely [32]. As a result, the transient signal is affected by larger instability and the determination might not be representative of the "average" concentration in the sample.

3.4. Methodologies comparison

Figs. 4 and 5 show a comparison of the performance of ICP-MS/MS applied to dissolved samples obtained through microwave-assisted acid digestion (green color) with LA-ICP-MS for the determination of REEs concentrations in manganese ores and slags (gold color). For LA-ICP-MS, two alternative approaches are evaluated, particularly relevant when complete sample dissolution is challenging: analysis of borate-fused glass beads prepared from raw powders (represented by a circle), and direct analysis of pressed powder pellets using an innovative calibration strategy that eliminates the need for matrix matching (represented by diamond shape).

Each elemental concentration axis is optimized around the mean value from all methodologies. In this representation error bars might look exaggerated, but instead the narrow range of variation in the

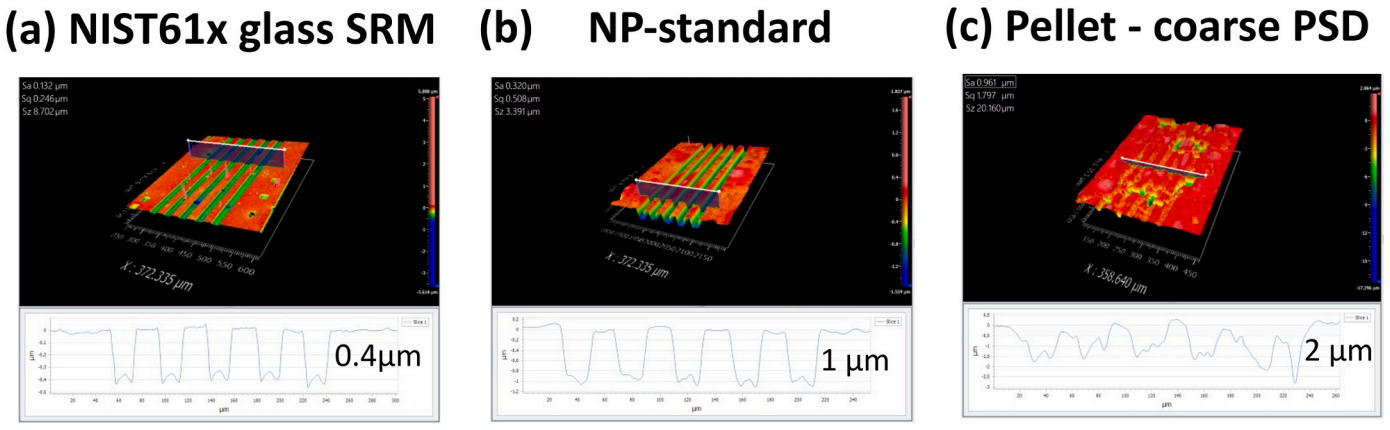

Fig. 3. White-light interferometry (WLI) determination of crater shape and depth of (a) NIST610 SRM, (b) NOD-A1 NP standard, and (c) a pressed pellet from coarse PSD (particle size distribution).

Table 6
LA-ICP-MS results of slags samples, using glass beads. Concentrations (C) are expressed in ppm (mg kg-1) with relative standard deviation expressed in %.

REE	Slag 1		Slag 2		Slag 3		Slag 4	
	C (mg kg^{-1})	RSD %	C (mg kg^{-1})	RSD %	C (mg kg^{-1})	RSD %	C (mg kg^{-1})	RSD %
Y	16.40	1.95	14.40	3.19	38.00	2.40	34.30	2.12
La	8.54	2.18	7.90	3.41	31.60	2.21	28.70	1.94
Ce	8.76	2.14	8.59	5.06	64.60	1.86	55.00	1.81
Pr	1.24	2.54	1.20	5.01	6.42	2.11	5.78	1.76
Nd	5.33	2.67	4.96	4.60	25.20	2.11	22.90	1.78
Sm	1.01	6.65	0.95	8.14	5.23	2.85	4.50	2.98
Eu	0.31	6.05	0.27	9.43	1.14	3.17	0.95	3.47
Gd	1.39	4.48	1.20	6.04	5.34	2.73	4.60	2.65
Tb	0.20	5.81	0.18	20.00	0.85	2.98	0.74	2.83
Dy	1.42	4.37	1.22	7.97	5.33	3.06	4.52	2.62
Ho	0.36	4.60	0.31	6.22	1.17	2.91	1.03	2.65
Er	0.89	6.33	0.78	8.09	3.16	3.48	2.79	3.11
Tm	0.14	7.32	0.12	10.28	0.45	3.55	0.43	3.56
Yb	0.98	5.90	0.89	7.93	2.86	3.51	2.66	3.45
Lu	0.16	5.60	0.14	8.17	0.46	3.33	0.40	3.37

Table 7
LA-ICP-MS results of Mn ores samples, using pressed pellets. Concentrations (C) are expressed in ppm (mg kg-1) with relative standard deviation expressed in %.

REE	Nchwaning lump		Zambian lump		SARM 16		SARM 17	
	C (mg kg^{-1})	RSD %	C (mg kg^{-1})	RSD %	C (mg kg^{-1})	RSD %	C (mg kg^{-1})	RSD %
Y	12.39	5.54	67.11	3.64	10.04	9.05	6.56	7.29
La	7.78	4.07	39.20	3.32	6.12	10.37	4.64	8.98
Ce	9.24	12.52	121.40	4.88	15.37	35.63	4.36	5.91
Pr	1.12	4.91	11.49	3.96	0.87	7.73	0.66	8.91
Nd	6.13	18.73	63.04	2.62	4.21	8.48	2.98	1.89
Sm	1.35	10.43	16.57	4.50	0.86	5.40	0.58	5.58
Eu	1.74	6.98	16.93	7.33	1.39	9.75	0.27	4.00
Gd	1.42	2.75	15.66	3.91	0.99	13.43	0.66	10.91
Tb	0.21	4.28	2.25	4.51	0.13	12.24	0.11	1.00
Dy	1.32	7.17	12.84	4.55	0.89	14.12	0.64	6.98
Ho	0.31	4.85	2.31	4.87	0.21	11.23	0.15	6.19
Er	0.88	4.44	6.23	4.51	0.66	6.64	0.50	9.94
Tm	0.12	10.00	0.86	5.86	0.09	15.25	0.07	20.00
Yb	0.83	3.21	5.27	5.33	0.61	7.93	0.45	14.50
Lu	0.13	6.79	0.72	5.42	0.09	6.06	0.06	11.76

Table 8
LA-ICP-MS results of slags samples, using glass beads. Concentrations (C) are expressed in ppm (mg kg-1) with relative standard deviation expressed in %.

REE	Slag 1		Slag 2		Slag 3		Slag 4	
	C (mg kg^{-1})	RSD %	C (mg kg^{-1})	RSD %	C (mg kg^{-1})	RSD %	C (mg kg^{-1})	RSD %
Y	7.09	12.40	51.44	5.69	35.07	6.07	35.62	5.69
La	10.23	12.97	41.35	7.03	28.51	4.79	28.63	7.03
Ce	1.35	12.71	94.87	10.01	68.94	8.10	65.68	10.01
Pr	5.14	11.16	9.81	8.07	6.83	5.76	6.79	8.07
Nd	0.98	8.71	37.75	6.16	26.70	4.04	26.14	6.16
Sm	0.48	17.04	8.15	5.29	5.78	4.49	5.65	5.29
Eu	0.83	6.79	1.68	13.26	1.74	9.57	1.68	13.26
Gd	0.18	4.26	6.68	7.18	4.61	5.27	4.63	7.18
Tb	1.27	11.75	1.07	8.30	0.75	5.82	0.74	8.30
Dy	0.37	14.74	7.00	4.21	4.79	5.01	4.85	4.21
Ho	0.95	12.27	1.53	12.39	0.97	6.15	1.06	12.39
Er	0.16	24.55	3.81	7.06	2.50	5.75	2.64	7.06
Tm	0.87	5.60	0.70	23.46	0.41	7.70	0.48	23.46
Yb	0.11	11.66	3.58	6.90	2.45	5.99	2.48	6.90
Lu	0.11	11.66	0.60	8.08	0.40	7.71	0.42	8.08

reported concentrations underscores the reliability, consistency, and strong agreement of the measurements among the various techniques used.

Carefully prepared samples, particularly those subjected to rigorous control of particle size and thorough homogenization, exhibited relative standard deviations within the 5–10 % range [33], with values near 5 % representing optimal analytical performance and those approaching 10 % remaining acceptable for quantitative purposes. In contrast, samples lacking a thorough homogenization step showed higher variability, with some RSD values reaching up to 20 % or higher [13,34]. Nevertheless, comparison with other analytical methodologies indicated that, although precision was reduced, the resulting measurements remained broadly accurate and aligned across methods. Elevated RSD values (10 % or higher) were also observed in cases where analyte concentrations approached the LLQ, reflecting the expected increase in variability near instrumental sensitivity thresholds.

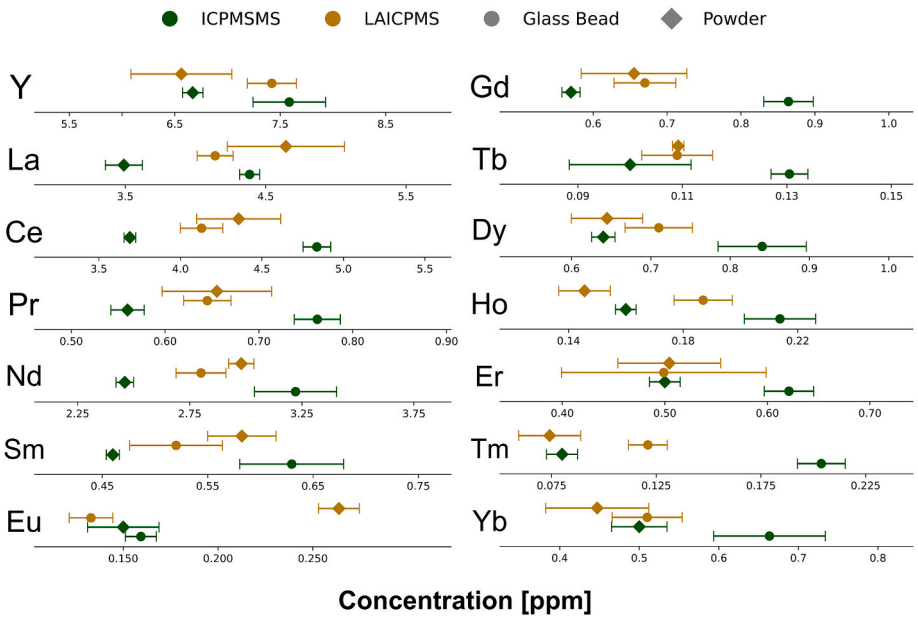

Fig. 4. Methodology comparison for sample SARM 17. Borate fusion sample preparation is represented by a circle shape, while use of powder is represented by diamond shape. The green and gold colors indicate ICP-MS/MS and LA-ICP-MS methodologies, respectively. (For interpretation of the references to color in this figure legend, the reader is referred to the Web version of this article.)

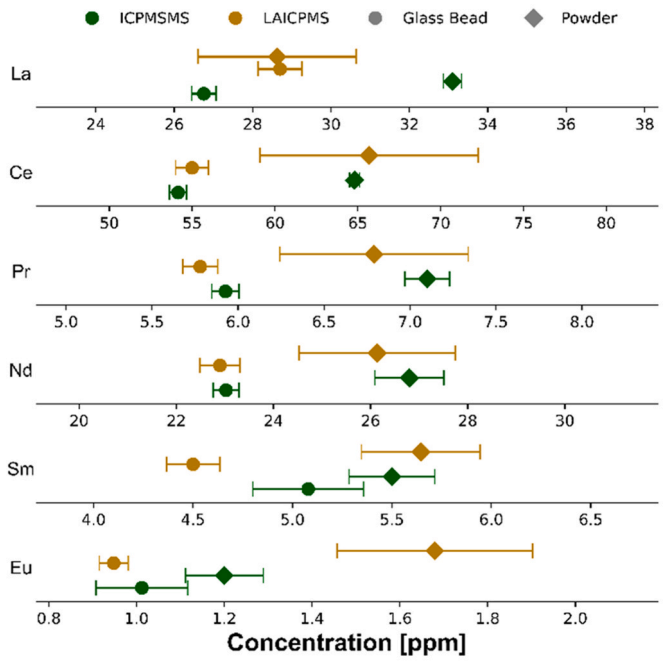

Fig. 5. Methodology comparison results for Slag 3. Borate fusion sample preparation is represented by a circle shape, while use of powder is represented by diamond shape. The green and gold colors indicate ICP-MS/MS and LA-ICP-MS methodologies, respectively. (For interpretation of the references to color in this figure legend, the reader is referred to the Web version of this article.)

As primary inspection tools, similar visualizations can be generated for each individual sample. Nevertheless, such an approach would be less effective for comparative analysis, especially if a larger number of samples need to be evaluated. Therefore, to gain a more comprehensive understanding and to systematically explore the differences across all samples, a statistical analysis is employed. This allows for a more rigorous and scalable evaluation of trends, outliers, and inter-sample variability.

3.4.1. *Mn ores statistical analysis*

Statistical analysis was conducted on manganese ore samples to evaluate the consistency of results across analytical methods. To assess potential discrepancies in elemental determination, an absolute relative bias metric can be applied, defined as:

$$\text{Absolute Relative Bias } (\%) = 100 \times \frac{|\text{Experimental Value} - \text{Reference Value}|}{\text{Reference Value}}$$

The analysis considered the entire set of concentrations for each method, combining data across all elements and samples. This approach provides a more direct measure of accuracy relative to standard reference values. Fig. 6 is a combination of heatmaps based on the absolute relative bias for all methodologies and satisfactory results are visible for all methods (plots are dominated by green hues, signaling a low discrepancy among groups) .

Laser ablation ICP-MS applied to pressed powder pellets (Fig. 6a) and to glass beads (Fig. 6b) showed generally good agreement with ICP-MS/MS measurements (Fig. 6c and d), with europium (Eu) being the only element exhibiting a consistent deviation. This discrepancy likely reflects matrix-dependent effects or limitations in calibration, given that the primary methodological difference between the two approaches—aside from sample preparation—was the use of triple-quadrupole technology in the ICP-MS/MS methods. Incorporating triple-quadrupole capabilities into LA-ICP-MS workflows could improve accuracy for Eu, especially in matrices with elevated BaO causing isobaric interferences. Although sample preparation strategies such as borate fusion enhance homogeneity and facilitate dissolution of refractory materials rich in Al_2O_3 or SiO_2, the results demonstrate that LA-ICP-MS of pressed pellets can still achieve performance comparable to more preparation-intensive techniques. Provided that laser fluence is maintained just above the ablation threshold and differences in ablation yield are properly corrected when using non-matrix-matched calibration [24], this approach offers a practical and efficient option for rapid, preliminary assessment of elemental concentrations in ore samples without the need for lengthy or complex preparation procedures.

3.4.2. *Slags samples statistical analysis*

For slags the difference among the methodologies varies significantly

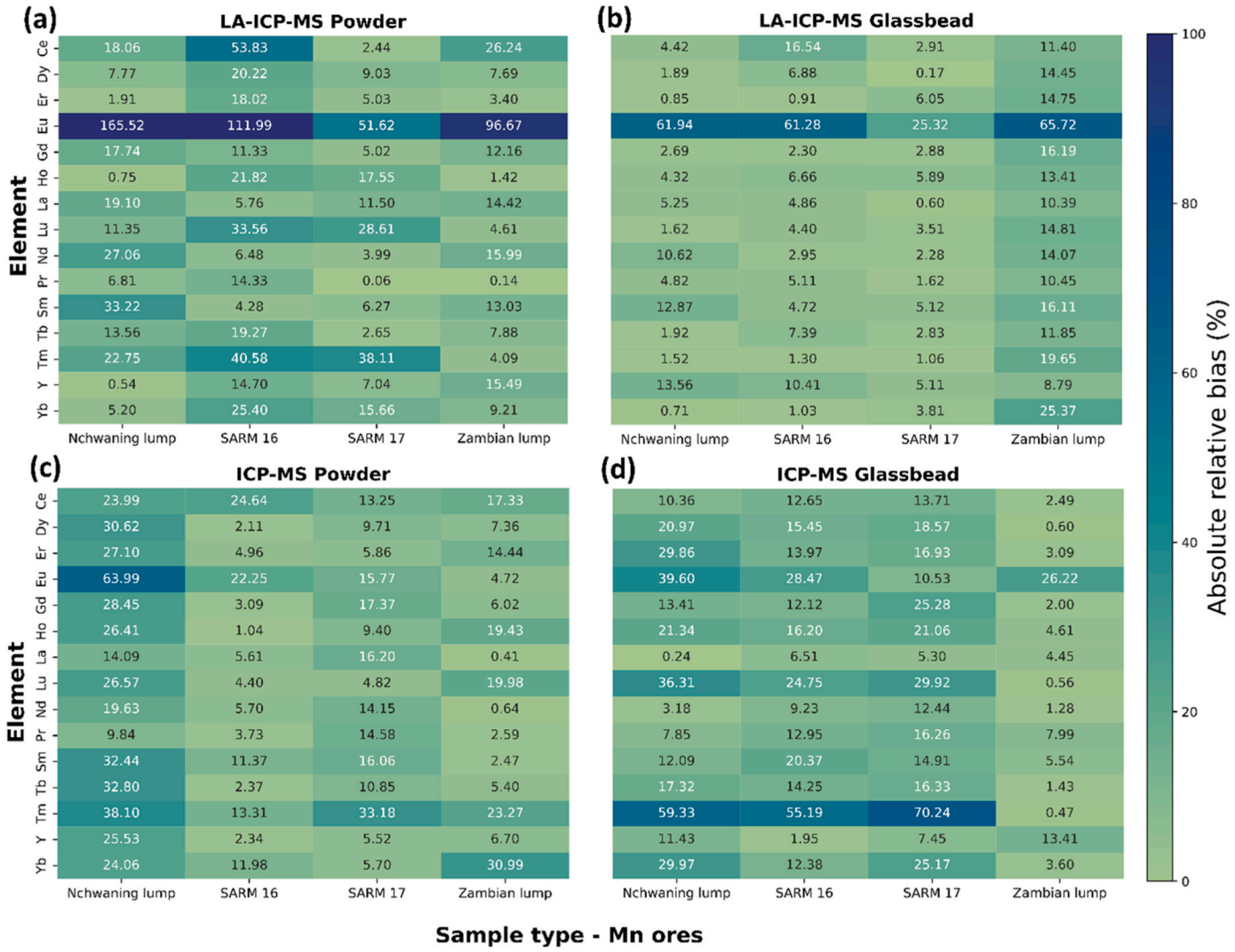

Fig. 6. Absolute relative bias for all elemental concentration and across all methodologies for Mn ores.

among the four samples, with some showing significant differences and other indicating comparable performance across methods.

Closer examination of Slag 1 and 2 using the absolute relative bias (Fig. 7), revealed substantial variability, largely driven by a single outlier technique skewing the population mean (LA-ICP-MS powder, visible also from Fig. S5 in SI).

Profilometric imaging of the LA-ICP-MS powder method for Slag 2 revealed more pronounced surface roughness than observed for glass reference materials, NP-standards, or Mn ore samples, reflecting its much coarser particle-size distribution. For this type of material, achieving optimal milling conditions and ensuring homogeneous trace-element distribution becomes considerably more difficult. In addition, accurate volume-based corrections become highly unreliable. Under these circumstances, direct analysis of pressed powders is discouraged.

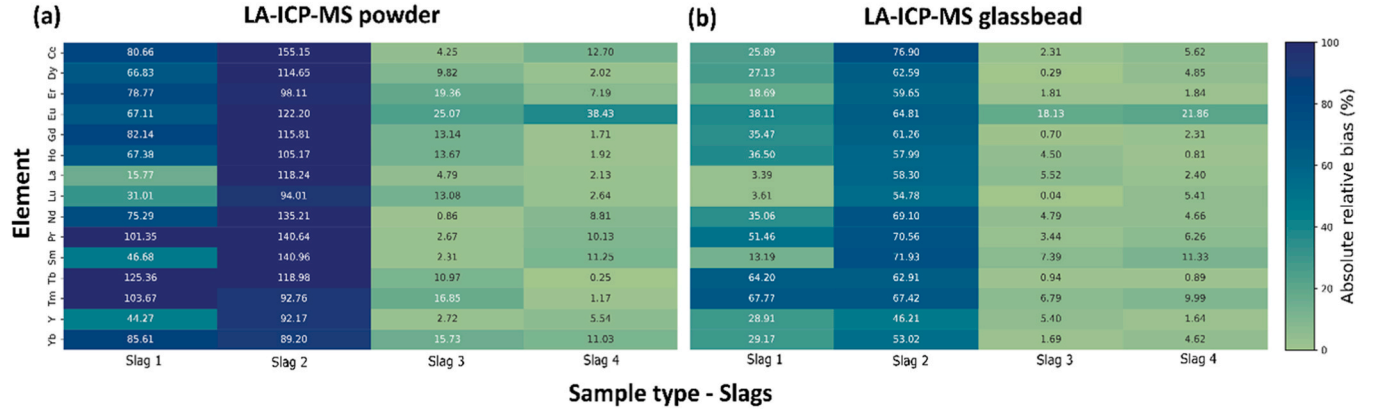

Fig. 7. Relative bias for all elemental concentration and across LA-ICP-MS methodologies for the sample type slags.

Instead, borate fusion is recommended to obtain a more homogeneous sample matrix and ensure robust analytical performance.

That is, however, not the case for all samples. In the case of Slag 3 and 4, the absolute relative bias between methods does not differ considerably. Although values for LA-ICP-MS on powder present a larger uncertainty, the absolute relative bias presents values of maximum 10 % and still predict reasonably well the concentration range of the elements of interest (Fig. 5).

4. Conclusions

The findings of this study underscore the critical role of sample morphology in selecting appropriate analytical strategies, as surface characteristics can significantly impact accuracy and reproducibility in LA-ICP-MS measurements.

The results from the Mn ores demonstrate that LA-ICP-MS non-matrix matched analysis on pelletized powder is a suitable method for analysis of solid samples without the need for specific SRMs, which are often unavailable for some of the matrices analyzed.

A relevant condition in the non-matrix matched approach is the selections of a laser fluence just above the ablation threshold and careful correction in ablation yield, since an increase in laser energy density leads to a steep increase in the gas fraction [35]. Although laser-induced fractionation is a known phenomenon, several elements previously attributed mainly to laser-induced fractionation are in fact significantly more impacted by ICP-induced, mass-load-dependent matrix effects [36], meaning that careful control of mass loading and a more homogeneously distributed plume can significantly reduce this effect.

This approach was further validated through interlaboratory comparison involving three different research institutions and three analytical methodologies, which demonstrated strong agreement in concentration values, even at lower ranges. When surface roughness or irregular morphology compromises reliable calibration, direct analysis of pressed powders becomes unsuitable. In such cases, the recommended approach is to employ borate fusion to produce glass beads prior to LA-ICP-MS analysis, ensuring improved precision and consistency across measurements.

For complex matrices such as slags, where particle size distribution is difficult to control, LA-ICP-MS on borate-fused glass beads proved to be the most reliable approach. This strategy offers an additional advantage: the same glass bead can be used for XRF analysis, which is commonly employed for major element determination, thereby streamlining workflows. Direct analysis of raw powders remains an interesting alternative when elements of interest are prone to volatilization during borate fusion.

Moving forward, these methodological advances are crucial for improving the mapping of critical raw materials in secondary resources, such as tailings. Accurate characterization enables economically viable recovery strategies by reducing dependence on primary mining and lowering operational costs. At the same time, optimizing the use of secondary resources minimizes waste generation, decreases CO_2 emissions, and supports circular economy principles. By unlocking the potential of tailings as alternative sources of strategic and critical elements, these approaches deliver a dual benefit: cost-effective resource utilization and significant progress toward sustainable industrial practices.

CRediT authorship contribution statement

Debora Foppiano: Writing – review & editing, Writing – original draft, Supervision, Project administration, Methodology, Investigation, Formal analysis, Data curation, Conceptualization. **Einar Jonsson:** Writing – review & editing, Methodology, Investigation. **Sarina Bao:** Writing – review & editing, Resources. **Øyvind Skår:** Writing – review & editing, Methodology, Investigation, Data curation. **Trond Slagstad:** Writing – review & editing, Resources, Funding acquisition. **Pankaj Kumar:** Writing – review & editing, Investigation. **Maria Wallin:** Writing – review & editing, Resources, Project administration, Funding acquisition. **Kristina Mervič:** Writing – review & editing, Methodology, Investigation, Data curation. **Martin Šala:** Writing – review & editing, Writing – original draft, Supervision, Resources, Project administration, Methodology, Investigation, Funding acquisition. **Casper van der Eijk:** Writing – review & editing, Project administration, Funding acquisition.

Declaration of competing interest

The authors declare that they have no known competing financial interests or personal relationships that could have appeared to influence the work reported in this paper.

Acknowledgments

The authors would like to acknowledge all funding schemes. A first part of the analyses for this study was performed in two nodes of the Norwegian Laboratory for Mineral and Materials Characterization (MiMaC). NGU node contribution was supported by the Research Council of Norway project number 269842/F50. SINTEF node contribution and NTNU contribution were supported by Horizon Europe project HAlMan (grant ref 101091936). The remaining part of the analyses was conducted at the National Institute of Chemistry in Ljubljana (Slovenia) and their contribution was supported by the Slovenian Research and Innovation Agency ARIS research core fundings no. P1-0034 and no. P2-0152. We also thank Nemko Norlab (Norway) for the XRF determinations. The graphical abstract for this publication was created in BioRender https://BioRender.com/tznz2co.

Appendix A. Supplementary data

Supplementary data to this article can be found online at https://doi.org/10.1016/j.talanta.2026.129478.

Data availability

Data will be made available on request.

References

[1] G. Gaustad, E. Williams, A. Leader, Rare earth metals from secondary sources: review of potential supply from waste and byproducts, Resour. Conserv. Recycl. 167 (2021) 105213, https://doi.org/10.1016/j.resconrec.2020.105213.
[2] European critical raw materials act - European commission, n.d. https://commission.europa.eu/topics/competitiveness/green-deal-industrial-plan/european-critical-raw-materials-act_en. (Accessed 16 November 2025).
[3] M. Grohol, C. Veeh, European Commission: Directorate-General for Internal Market, Industry, Entrepreneurship and SMEs, Study on the Critical Raw Materials for the EU 2023 – Final Report, Publ. Off. Eur. Union, 2023. https://data.europa.eu/doi/10.2873/725585.
[4] J. Safarian, A sustainable process to produce manganese and its alloys through hydrogen and aluminothermic reduction, Processes 10 (2021), https://doi.org/10.3390/pr10010027.
[5] A. Sarkar, T.L. Schanche, M. Wallin, J. Safarian, Kinetics study on the H2 reduction of nchwaning manganese ore at elevated temperatures, Int. J. Min. Met. Mater. 32 (2025) 1091–1102, https://doi.org/10.1007/s12613-025-3094-x.
[6] S. Bao, C. van der Eijk, D. Foppiano, Characterisation of manganese ores and slags for production of ferromanganese and Al-Mn master alloys, in: 17th Int. Ferroalloy INFACON XVII, People's Republic of China, Beijing, 2024, pp. 383–394. https://hdl.handle.net/11250/3185371. (Accessed 1 December 2025).
[7] L. Brunnbauer, Z. Gajarska, H. Lohninger, A. Limbeck, A critical review of recent trends in sample classification using laser-induced breakdown spectroscopy (LIBS), TrAC, Trends Anal. Chem. 159 (2023), https://doi.org/10.1016/j.trac.2022.116859.
[8] J. Malherbe, F. Claverie, A. Alvarez, B. Fernandez, R. Pereiro, J.L. Molloy, Elemental analyses of soil and sediment fused with lithium borate using isotope dilution laser ablation-inductively coupled plasma-mass spectrometry, Anal. Chim. Acta 793 (2013) 72–78, https://doi.org/10.1016/j.aca.2013.07.031.
[9] F.P. Leitzke, A.C. Wegner, C.C. Porcher, N.I.M. Vieira, J. Berndt, S. Klemme, R. V. Conceição, Whole-rock trace element analyses via LA-ICP-MS in glasses produced by sodium borate flux fusion, Braz. J. Geol. 51 (2021) e20200057, https://doi.org/10.1590/2317-4889202120200057.
[10] R.M. Conrey, D.G. Bailey, J.W. Singer, L.J. Wagoner, B. Parfitt, J. Hay, O. Keh, Z. Chang, S. Huang, Combined use of multiple external and internal standards in

LA-ICP-MS analysis of bulk geological samples using lithium borate fused glass, Geochem. Explor. Environ. Anal. 23 (2023), https://doi.org/10.1144/geochem2023-001 geochem2023-001.
[11] L. Guldris Leon, J.L. Thauront, K.J. Hogmalm, E. Hulthén, J. Malmqvist, Evaluation of refractory metal concentrations in nano-particulate pressed-powder pellets using LA-ICP-MS, Minerals 12 (2022), https://doi.org/10.3390/min12070869.
[12] D. Yang, K. Tanilas, A. Konist, O. Järvik, Evaluating LA-ICP-MS and digestion-based ICP-MS methods for trace elements determination in oil shale and its solid wastes, Talanta 295 (2025) 128319, https://doi.org/10.1016/j.talanta.2025.128319.
[13] A. Limbeck, P. Galler, M. Bonta, G. Bauer, W. Nischkauer, F. Vanhaecke, Recent advances in quantitative LA-ICP-MS analysis: challenges and solutions in the life sciences and environmental chemistry, (n.d.). https://doi.org/10.1007/s00216-015-8858-0.
[14] D. Chew, K. Drost, J.H. Marsh, J.A. Petrus, LA-ICP-MS imaging in the geosciences and its applications to geochronology, Chem. Geol. 559 (2021) 119917, https://doi.org/10.1016/j.chemgeo.2020.119917.
[15] K. Mervič, M. Šala, S. Theiner, Calibration approaches in laser ablation inductively coupled plasma mass spectrometry for bioimaging applications, TrAC, Trends Anal. Chem. 172 (2024) 117574, https://doi.org/10.1016/j.trac.2024.117574.
[16] N. Saberi, B. Vriens, Compositional heterogeneity of secondary minerals in mine waste rock: origins and implications for water quality, J. Hazard. Mater. 487 (2025) 137163, https://doi.org/10.1016/j.jhazmat.2025.137163.
[17] R.E. Russo, X. Mao, J.J. Gonzalez, V. Zorba, J. Yoo, Laser ablation in analytical chemistry, Anal. Chem. 85 (2013) 6162–6177, https://doi.org/10.1021/ac4005327.
[18] S.H. Jeong, O.V. Borisov, J.H. Yoo, X.L. Mao, R.E. Russo, Effects of particle size distribution on inductively coupled plasma mass spectrometry signal intensity during laser ablation of glass samples, Anal. Chem. 71 (1999) 5123–5130, https://doi.org/10.1021/ac990455a.
[19] J. Pisonero, B. Fernández, D. Günther, Critical revision of GD-MS, LA-ICP-MS and SIMS as inorganic mass spectrometric techniques for direct solid analysis, J. Anal. At. Spectrom. 24 (2009) 1145, https://doi.org/10.1039/b904698d.
[20] H. Hu, J. Zhou, Y. Ye, H. Li, C. Tu, H. Wen, Y. Ke, Y. Sun, Preparation of REE-doped CaF2 single crystals for accurate determination of REE concentrations in CaF2 crystals via UV-LA-ICP-MS, Talanta 285 (2025) 127393, https://doi.org/10.1016/j.talanta.2024.127393.
[21] S. Balachandar, W. Zhang, Y. Liu, Z. Hu, H. Chen, T. Luo, T. He, X. Zeng, Bulk analysis of columbite ores by LA-ICP-MS: development of reference materials and investigation into matrix effects, J. Anal. At. Spectrom. 40 (2025) 259–275, https://doi.org/10.1039/D4JA00311J.
[22] Z. Tang, S. Chen, D. Zhao, T. Zhang, Y. Ge, Z. Li, R. Zhang, L. Zhou, Accurate high-resolution LA-ICP-MS determination of trace element contents in carbonates with matrix-matched standards, J. Anal. At. Spectrom. 40 (2025) 3256–3265, https://doi.org/10.1039/D5JA00333D.
[23] K. Mervič, V.S. Šelih, M. Šala, J.T. Van Elteren, Non-matrix-matched calibration in bulk multi-element laser ablation – inductively coupled plasma – mass spectrometry analysis of diverse materials, Talanta 271 (2024) 125712, https://doi.org/10.1016/j.talanta.2024.125712.
[24] K. Mervič, J.T. Van Elteren, M. Bele, M. Šala, Utilizing ablation volume for calibration in LA-ICP-MS mapping to address variations in ablation rates within and between matrices, Talanta 269 (2024) 125379, https://doi.org/10.1016/j.talanta.2023.125379.
[25] P. Kumar, J. Safarian, Sustainable production of ultra-low-carbon ferromanganese and calcium aluminate slag from pre-reduced manganese ore using aluminium, Can. Metall. Q. 0 (2025) 1–22, https://doi.org/10.1080/00084433.2025.2587792.
[26] S.M. Eggins, Laser ablation ICP-MS analysis of geological materials prepared as lithium borate glasses, Geostand. Newsl. 27 (2003) 147–162, https://doi.org/10.1111/j.1751-908X.2003.tb00642.x.
[27] D. Günther, A.v. Quadt, R. Wirz, H. Cousin, V.J. Dietrich, Elemental analyses using laser ablation-inductively coupled plasma-mass spectrometry (LA-ICP-MS) of geological samples fused with Li2B4O7 and calibrated without matrix-matched standards, Microchim. Acta 136 (2001) 101–107, https://doi.org/10.1007/s006040170038.
[28] B. Flem, R.B. Larsen, A. Grimstvedt, J. Mansfeld, In situ analysis of trace elements in quartz by using laser ablation inductively coupled plasma mass spectrometry, Chem. Geol. 182 (2002) 237–247, https://doi.org/10.1016/S0009-2541(01)00292-3.
[29] S.J.M.V. Malderen, A.J. Managh, B.L. Sharp, F. Vanhaecke, Recent developments in the design of rapid response cells for laser ablation-inductively coupled plasma-mass spectrometry and their impact on bioimaging applications, J. Anal. At. Spectrom. 31 (2016) 423–439, https://doi.org/10.1039/C5JA00430F.
[30] B. Paul, J. Petrus, D. Savard, J. Woodhead, J. Hergt, A. Greig, C. Paton, P. Rayner, Time resolved trace element calibration strategies for LA-ICP-MS, J. Anal. At. Spectrom. 38 (2023) 1995–2006, https://doi.org/10.1039/D3JA00037K.
[31] D. Chetty, J. Gutzmer, REE redistribution during hydrothermal alteration of ores of the Kalahari Manganese Deposit, Ore Geol. Rev. 47 (2012) 126–135, https://doi.org/10.1016/j.oregeorev.2011.06.001.
[32] A. Jerše, K. Mervič, J.T. van Elteren, V.S. Šelih, M. Šala, Quantification anomalies in single pulse LA-ICP-MS analysis associated with laser fluence and beam size, Analyst 147 (2022) 5293–5299, https://doi.org/10.1039/D2AN01172G.
[33] C. D'oriano, S. Dapelo, F. Podda, R. Cioni, Laser-ablation inductively coupled plasma mass spectrometry (LA-ICP-MS): setting operating conditions and instrumental performance, period, Minerals 77 (2008) 65–74, https://doi.org/10.2451/2008PM0019.
[34] M. De Bruin-Hoegée, J. Schoorl, P. Zoon, M.J. Van Der Schans, D. Noort, A.C. Van Asten, A novel standard for forensic elemental profiling of polymers by LA-ICP-TOF-MS, Forensic Chem. 35 (2023) 100515, https://doi.org/10.1016/j.forc.2023.100515.
[35] T. Van Helden, K. Mervič, I. Nemet, J.T. Van Elteren, F. Vanhaecke, S. Rončević, M. Šala, T. Van Acker, Evaluation of two-phase sample transport upon ablation of gelatin as a proxy for soft biological matrices using nanosecond laser ablation – inductively coupled plasma – mass spectrometry, Anal. Chim. Acta 1287 (2024) 342089, https://doi.org/10.1016/j.aca.2023.342089.
[36] I. Kroslakova, D. Günther, Elemental fractionation in laser ablation-inductively coupled plasma-mass spectrometry: evidence for mass load induced matrix effects in the ICP during ablation of a silicate glass, J. Anal. At. Spectrom. 22 (2006) 51–62, https://doi.org/10.1039/B606522H.